







# Model Predictive MRAS Speed Estimator for Permanent Magnet Synchronous Machines

Saleh B. Shlimet D | Antonio Griffo

Department of Electronic and Electrical Engineering, The University of Sheffield, Sheffield, UK

Correspondence: Saleh B. Shlimet (salehhoba78@gmail.com)

Received: 18 March 2025 | Revised: 10 September 2025 | Accepted: 26 October 2025

#### **ABSTRACT**

This paper presents a predictive model reference adaptive system (MRAS) speed estimator for permanent magnet synchronous machines. The speed estimator is based on the finite control set model predictive control principle. A search method is utilized to find the best estimated speed at each sampling interval that produces the smallest speed estimation error signal. This method replaces the PI controller which is typically employed by MRAS estimators. The speed estimator has been experimentally tested using a 2.1 kW PMSM. Results show improved performance, especially during fast load transients for the novel method compared to the PI-based MRAS method.

## 1 | Introduction

The use of permanent magnet synchronous machines (PMSM) is widespread in both industrial and high-performance applications such as electric vehicles traction, thanks to their high efficiency, high power density, and simple structure [1]. PMSMs are typically controlled using field-oriented control due to its high accuracy and fast dynamics. Accurate rotor position measurement is required for field orientation, and encoders or resolvers are used to provide the rotor position data. In low-cost applications, the additional cost, size, weight, as well as the additional wiring and associated electronics components of position sensors are undesirable, resulting in continuous interest in sensorless control systems. In high performance applications, where reliability is a critical requirement, such as EV traction motors where resolvers are typically used, sensorless estimation is often a requirement as a backup solution in case of sensor failure, in order to increase drive reliability and availability [2]. To address issues with the use of sensors, sensorless control strategies have been extensively studied. Model Reference Adaptive System (MRAS)-based estimators are one of the most popular sensorless position estimation methods [3]. Due to its simple design and good performance over a large speed range, the fixed-gain PI controller is frequently employed in the MRAS schemes' adaptation mechanism to obtain the estimated speed. However, as inverter nonlinearities and machine parameter variation become more prevalent at low speeds, it might not offer the desired performance over the full speed operating range. Furthermore, tuning the PI gains may require effort through trial-and-error procedures.

Many solutions have been proposed to replace the fixed PI controller with more advanced algorithms. [4, 5] suggested replacing the PI adaptation mechanism with a sliding mode (SM) algorithm. Although these methods enhance the dynamic response of the estimator and resilience to parameter fluctuations, the chattering issue and the position accuracy is undermined by high-order harmonics and external noise during the estimation of fundamental back-EMF, especially in dynamic conditions [6, 7]. To solve the problems mentioned above, [8] introduced an improved SMO using a sigmoid function. However, the accuracy of speed estimation during transient period suffered because of DC offsets. A voltage model observer-based SMO proposed by [9] to address the problem of DC offsets that lead to a deterioration in speed estimation. Recent works have focused on improving sliding-mode-based sensorless control. An improved SMO with exponential input and a disturbance observer has

This is an open access article under the terms of the Creative Commons Attribution License, which permits use, distribution and reproduction in any medium, provided the original work is properly cited.

@ 2025 The Author(s). The Journal of Engineering published by John Wiley & Sons Ltd on behalf of The Institution of Engineering and Technology.

been shown to reduce chattering and enhance robustness, while fuzzy dual sliding-mode MRAS methods use fuzzy logic to adaptively tune gains for better accuracy under parameter uncertainty. Both approaches improve estimation performance but at the expense of higher system complexity [10, 11]. More recently, [12] introduced a fuzzy integral terminal sliding-mode observer (FITSMO) for PMSM sensorless control. This method achieves finite-time convergence of estimation error and adaptively adjusts sliding-mode gains using fuzzy logic, leading to improved robustness and position accuracy under varying operating conditions. However, the approach requires careful tuning of fuzzy membership functions and control parameters, and the combined fuzzy-sliding mode structure increases computational complexity. A fast super twisting algorithm-based sliding mode improved MRAS observer (FSTA-SM-IMRASO) by [13], enhances conventional MRAS by adding a feedback correction term and adaptive gain to improve error convergence. A fast super twisting algorithm with an exponential term replaces the PI controller, achieving faster convergence and improved robustness under parameter variations and disturbances. However, it still suffers from residual chattering, requires careful tuning of slidingmode and adaptive feedback parameters, and has a complex structure.

Artificial neural networks (ANNs) have been introduced in sensorless control to replace the conventional PI controller in MRAS schemes, offering improved adaptability and robustness against parameter variations. [14] Introduced an ANN-based sensorless direct torque control (DTC) scheme, demonstrating improved dynamic torque response and reliable sensorless operation. However, the approach increases computational complexity and requires careful network training.

Predictive control controllers (MPCs) for sensorless applications have attracted a lot of attention recently, and they are divided into two categories: classical MPCs, where the controller generates a continuous output that is applied to the system via a modulator, and finite control set-model predictive controllers (FCS-MPCs), where the controller selects the optimal control action from a finite table of potential output states [15]. Due to its ease of use and ability to incorporate any performance specifications, FCS-MPC has been used in a wide range of applications [16]. A sensorless induction machine control system with a predictive current controller was suggested in [17], and it strengthens the robustness against changes in motor parameters. In [18], speed and current predictive controllers for a sensorless PMSM drive system were presented, achieving fast transient responses and good tracking performance. An FSC-MPC was used in [19] to drive an IM fed by a matrix converter in order to increase system efficiency, and in [20] a proposed control scheme based on predictive deadbeat algorithm showed an excellent performance for a sensorless vector-controlled PMSG, and satisfactory robustness against changes in parameters.

Unlike the abovementioned MPCs, [21] introduced a FS-MPC-based position estimator for IM where the prediction principle was applied on the design of the position estimator rather than to the current or speed control of the drive. A rotor position search algorithm was used to obtain the optimal position corresponding to minimum cost function at each sampling time, eliminating the need for PI controller.

In this paper, a FCS-MPC-based speed estimator is introduced. In this scheme, the adaptation mechanism is based on solving an optimization problem with the aim of minimizing, the speed tuning error signal of the estimator over a finite number of potential rotor speeds. A rotor speed search algorithm is used to ensure that the optimal speed is obtained at each sampling time. The algorithm in this method differs from the one proposed in [21], which searches for the optimum position. In contrast, the speed search-based method can be implemented into MRAS methods, where the adaptive model is a function of both speed and position. However, in the position searchbased method, the adaptive model must be solely a function of position to ensure compatibility. Unlike advanced methods such as FSTA-SM-IMRASO, the proposed FCS-MPC-based MRAS offers a simpler design, as it does not rely on manually tuned gains. The control action is obtained directly by minimizing a cost function, eliminating gain tuning, reducing implementation effort, and improving robustness across varying operating conditions. Its execution time is sufficiently low for implementation on low-cost controllers, providing a favourable trade-off between performance, robustness, and computational efficiency The performance of the speed search-based estimator was implemented and evaluated against the proposed PWM-based estimator (PIbased flux MRAS). Results show the superior performance of the predictive method particularly during transient period.

## 2 | Machine Model

The voltage equations of a PMSM can be represented in the estimated rotating dq-reference frame as:

$$L_{d} \frac{\mathrm{d}\hat{i}_{d}}{\mathrm{d}t} = \hat{v}_{d} - R\hat{i}_{d} + \hat{w}\left(\hat{\psi}_{m_{q}} + L_{q}\hat{i}_{q}\right) \tag{1}$$

$$L_q \frac{\mathrm{d}\hat{i}_q}{\mathrm{d}t} = \hat{v}_q - R\hat{i}_q - \hat{w}\left(\hat{\psi}_{m_d} + L_d\hat{i}_d\right) \tag{2}$$

where  $\hat{v}_d$ ,  $\hat{v}_q$ ,  $\hat{l}_d$ ,  $\hat{l}_q$  are estimated dq-axis voltages and currents, respectively;  $L_d$ ,  $L_q$ , R are the dq-axis inductances as well as the stator resistance,  $\hat{w}$  is the estimated rotor speed,  $\hat{\psi}_{m_q}$  is the flux on estimated q-axis. and  $\hat{\psi}_{m_d}$  is the rotor PM flux linkage on the estimated  $\hat{d}$ -axis.

## 3 | PWM-Based Speed Estimator

Considering the standard space-vector PWM switching period in a voltage-source inverter, four voltage vectors are applied in sequence, including two active and two zero vectors. The time instants when these are applied can be indicated as  $t_1 \cdots t_8$ , for example,  $t_1$  and  $t_8$  are the time instants at which the zero vectors  $V_0$  and  $V_7$  are applied respectively. By discretizing Equation (1) with a sampling time  $T_{\rm s}$ , the resultant relationships between two adjacent sampling points, are given as:

$$\hat{v}_{d(t_1 \sim (t_1 + T_s))} = R \hat{i}_{d(t_1 \sim (t_1 + T_s))} + L_d \frac{d}{dt} \hat{i}_{d(t_1 \sim (t_1 + T_s))} - \hat{w} L_q \hat{i}_{q(t_1 \sim (t_1 + T_s))} - \hat{w} \hat{v}_{m_q}$$
(3)

$$\begin{split} \widehat{v}_{d((t_1+(n-2)T_s)\sim t_8)} &= R \hat{i}_{d((t_1+(n-2)T_s)\sim t_8)} + L_d \frac{d}{dt} \hat{i}_{d(t_1+(n-2)T_s)\sim t_8)} \\ &- \hat{w} L_q \hat{i}_{q((t_1+(n-2)T_s)\sim t_8)} - \hat{w} \hat{\psi}_{m_q} \end{split} \tag{4}$$

Where  $t_1$  is the beginning of the PWM period, n is the integer number of sampling points in one switching period,  $t_8 = t_1 + (n-1)T_s$ .

The derivative term can be obtained as:

$$\frac{d}{dt}\hat{i}_{d} = (\hat{i}_{d(t_{1}+(k+1)T_{s})} - \hat{i}_{d(t_{1}+kT_{s})})/T_{s}$$
 (5)

By assuming that  $\hat{w}$  is constant during one switching period, and multiplying the n-1 equations by  $T_s$  and adding each equation to the next, it yields:

$$T_{s} \sum_{1}^{n-1} \hat{v}_{d(j)} = T_{s} R \sum_{1}^{n-1} \hat{i}_{d(j)} - t_{s} \hat{w} \hat{\psi}_{m_{q}} - \hat{w} T_{s} L_{q} \sum_{1}^{n-1} \hat{i}_{q(j)}$$

$$+ L_{d} \sum_{1}^{n-1} \left( \hat{i}_{d(k+1)} - \hat{i}_{d(k)} \right)$$

$$(6)$$

Where  $t_{sw} = 1/f_{sw}$ ,  $f_{sw}$  is the switching frequency, j is the jth equation and k = 0, 1... n - 2.

According to [22],  $T_s \sum_{1}^{n-1} \hat{v}_d(j)$  is equal to the average PWM output voltage:

$$(t_3 - t_2)\hat{v}_{d(t_3 - t_2)} + (t_4 - t_3)\hat{v}_{d(t_4 - t_3)} + (t_6 - t_5)\hat{v}_{d(t_6 - t_5)}$$

$$+ (t_7 - t_6)\hat{v}_{d(t_7 - t_6)} = T_s \sum_{1}^{n-1} \hat{v}_{d(j)}$$

$$(7)$$

Where  $\hat{v}_{d(t_3-t_2)}$ ,  $\hat{v}_{d(t_4-t_3)}$ ,  $\hat{v}_{d(t_6-t_5)}$  and  $\hat{v}_{d(t_7-t_6)}$  are the switching vectors on the estimated d-reference frame.

As the switching period consists of two symmetrical switching combinations, it can be proven that:

$$(t_3 - t_2) \,\hat{v}_{d(t_2 - t_2)} = (t_7 - t_6) \,\hat{v}_{d(t_2 - t_6)} \tag{8}$$

$$(t_4 - t_3) \,\hat{v}_{d(t_4 - t_2)} = (t_6 - t_5) \,\hat{v}_{d(t_6 - t_5)} \tag{9}$$

Therefore, Equation (7) now becomes:

$$2\left[(t_3 - t_2) * \hat{v}_{d(t_3 - t_2)} + (t_4 - t_3) * \hat{v}_{d(t_4 - t_3)}\right] = T_s \sum_{1}^{n-1} \hat{v}_{d(j)}$$
 (10)

Substitute Equation (10) into Equation (6) and rearrange to calculate  $\hat{\psi}_{m_a}$  for vector controlled PMSM drive ( $i_d = 0$ )

$$\hat{\psi}_{m_q} = \frac{f_{\text{sw}}}{\hat{w}} \left[ -2\left( (t_3 - t_2) * \hat{v}_{d(t_3 - t_2)} + (t_4 - t_3) * \hat{v}_{d(t_4 - t_3)} \right) - \hat{w} T_s L_q \sum_{1}^{n-1} \hat{\mathbf{i}}_{q(j)} \right]$$
(11)

The switching vectors  $\hat{v}_{d(t_3-t_2)}$ ,  $\hat{v}_{d(t_4-t_3)}$  and the time differences  $(t_3-t_2)$  and  $(t_4-t_3)$  are calculated at the beginning of the PWM

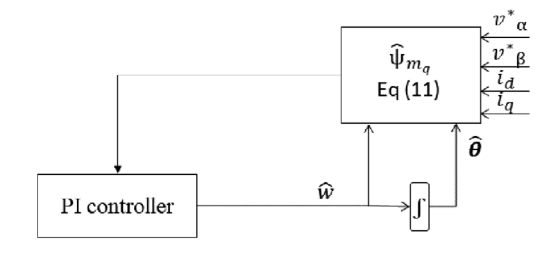
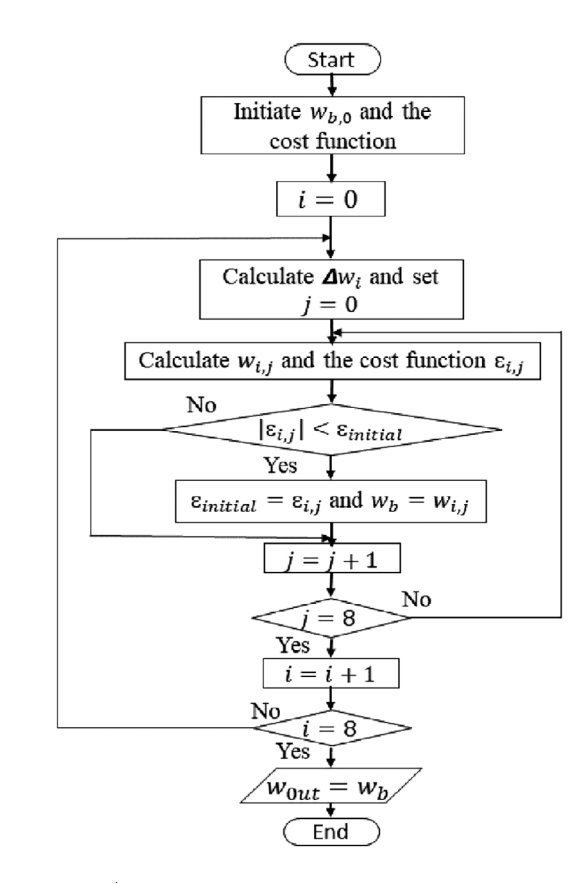


FIGURE 1 | Block diagram of the PI-based MRAS estimator.



**FIGURE 2** | Flowchart of the rotor speed search algorithm.

period based on the location of the rotating voltage reference vector on the space vector diagram. Therefore, the voltage reference on  $\alpha\beta$  frame  $(v^*_{\alpha}, v^*_{\beta})$  should take the form of a rotating space vector.

The actual flux is  $\psi_m$  on the real d-axis and 0 on the real q-axis, and the magnitude of the cross product of the flux components,  $\varepsilon$ , is fed into a PI controller to estimate the speed, which is then integrated to obtain the estimated position as shown in Figure 1.

$$\varepsilon = \psi_{m_d}.\hat{\psi}_{m_q} - \psi_{m_q}.\hat{\psi}_{m_d} = \psi_m.\hat{\psi}_{m_q}$$
 (12)

#### 4 | Predictive MRAS Estimator

The predictive rotor speed estimator is based on the FCS-MPC concept for designing the adaptation mechanism. The flowchart of the algorithm is illustrated in Figure 2, while the block diagram of the predictive estimator is depicted in Figure 3. The traditional MRAS minimizes the rotor flux error by utilizing a PI controller,

The Journal of Engineering, 2025

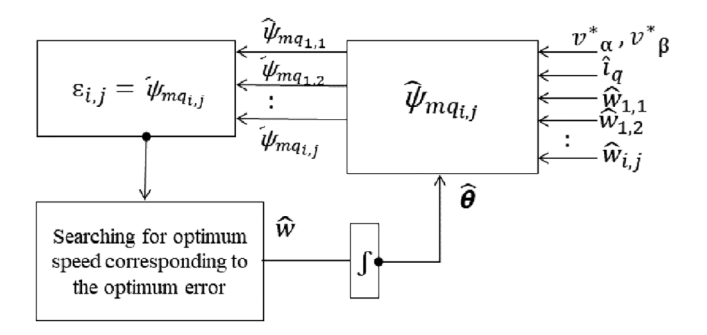


**FIGURE 3** | Block diagram of the predictive estimator.

whose output is the estimated speed  $\hat{\omega}$ . Similarly, in the proposed FCS-MPC-MRAS method, the estimated speed is the output of a minimization problem, which consists of minimizing a cost function proportional to the rotor flux error, by selecting the estimated speed from a finite set of options that is iteratively narrowed down until convergence is reached.

Since the rotor speed is a continuous signal, it is necessary to discretize it into a finite number of potential speeds to allow the evaluation of the cost function in a discrete number of steps as required by the finite control set MPC methodology. An algorithm is employed to discretize the rotor speed and calculate the cost function for each of these discrete speeds. The algorithm initiates by calculating the initial cost function at the starting speed ( $w_{b,0} = 0 \text{ rad/s}$ ). The discretization of the speed begins by starting from the initial speed and then displacing this speed by a displacement ( $\Delta w_i$ ) which is calculated as follows:

$$\Delta w_i = 236 \cdot 2^{-i} \tag{13}$$

where i is the order of the iteration and 236 is chosen because the rated speed of the tested machine is approximately 944 rad/s in electrical. The displacement of the base speed ( $w_b$ ) is iterated to produce nine discrete rotor speeds as follows:

$$w_{i,j} = w_b + \Delta w_i.(j-4)$$
 (14)

where *j* is the order of the displacement =  $0 \cdots 8$ 

In the initial iteration (i=0),  $\Delta w_i=236$ . Applying Equation (14) will produce nine discrete speeds in electrical rad/s: 944, 708, 472, 236, 0, -236, -472, -708, and -944. Each of these discrete speeds is used to calculate the fluxes on estimated q-axis,  $\hat{\psi}_{m_q}$  in Equation (11), corresponding to each individual speed. Consequently, the cost function,  $\varepsilon_{i,j}$  in Equation (12), is calculated for each speed. The speed corresponding to the minimum cost function of the nine speeds is chosen as the base speed for the next iteration.

At the next iteration (i=1), the speed displacement is decreased to  $\Delta w_i = 236 \cdot 2^{-1} = 118$ , which increases the search accuracy by a factor of 2. The search starts again from the new base speed  $w_{b,1}$  to find the speed that generates the minimum cost function in the second iteration. After each iteration, the search algorithm gets closer to the optimal speed, and by the end of the tenth iteration ( $\Delta w_8 = 0.46$ ) the optimal speed can be found with 0.46 accuracy. Finally, the position is estimated by integrating the speed.

**TABLE 1** | Machine parameters.

Quantity	Unit	Value
Pole-pairs	_	3
Rated power	kW	2.1
Stator resistance	ohm	2.19
Rated current	A	4.2
Base speed	rpm	3000
Rated torque	Nm	6.7
Torque constant	Nm/A	1.6
PM flux linkage	V/Hz	0.356
d-axis inductance	mH	12.5
q-axis inductance	mH	15
Inertia	Kg m <sup>2</sup>	0.00077

As the rotor speed does not change significantly between two-time samples, the search algorithm can be initialized by the output of the algorithm at the end of the last sampling instant (previous output speed) without affecting the estimation accuracy. This considerably reduces the execution time of the algorithm from 8 to 3  $\mu s$  on the Speedgoat controller (1.99 GHz clock). Meanwhile, the TMS320F28335 microcontroller (150 MHz clock), which is a low-cost option, executes the algorithm in roughly 39  $\mu s$ , compared to roughly 15  $\mu s$  required for the classical method. To minimize execution time, sine and cosine functions in the reference frame transformations are replaced with a one-period look-up table, which executes much faster than standard high-level function calls.

A fixed gain PI controller may be unable to maintain optimal performance under all different operating conditions. At low speeds the PI gains need to be tuned to small values to prevent significant oscillations in the estimated speed. However, for the system to operate smoothly and satisfactorily during transient operation conditions, when a sudden change occurs in load or speed, the PI bandwidth and gains need to be increased. Therefore, an adaptive PI controller may be required for a satisfactory performance, however, this is a difficult process that requires trial and error. The effect of the PI controller gains on the estimated speed was experimentally tested in [23]. The results showed that by using high PI gains, the estimated speed oscillation increase, but implementing high gains improved the dynamic performance and had a faster response compared to the response when low PI gains were applied. Unlike PI-based MRAS methods the predictive method does not need any gain tuning, which makes it simpler and guarantees optimum performance.

### 5 | Simulation Results

The predictive method was tested for various conditions by using MATLAB/Simulink. It was assumed that neither the inverter nonlinearity nor the dead time effects were considered. The motor parameters are shown in Table 1. In Figure 4, the machine is tested at low speeds under 20% of rated torque. The reference speed initially set to 5 rad/s and then set to -5 rad/s at 0.5 s and then set

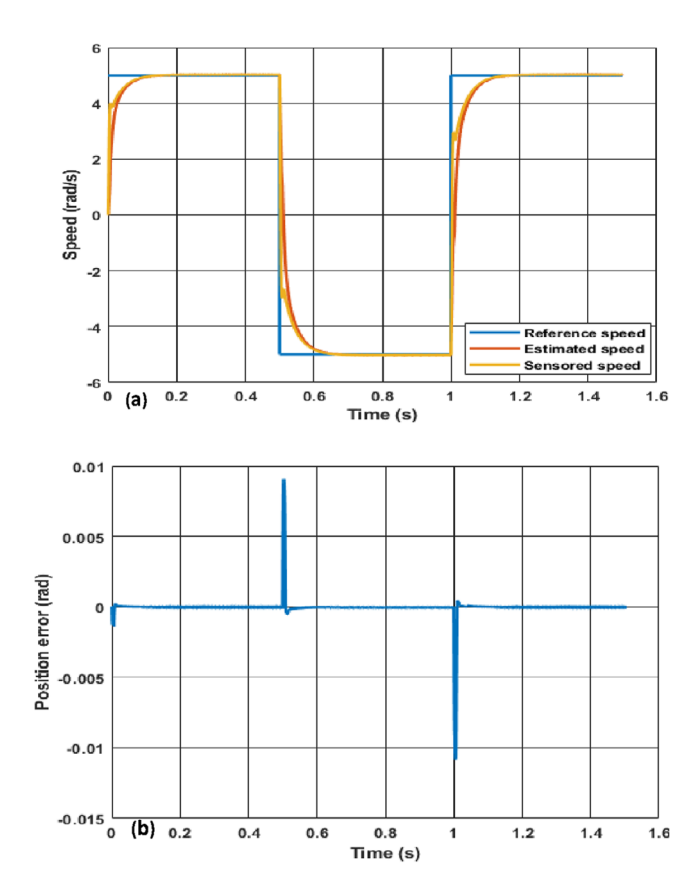
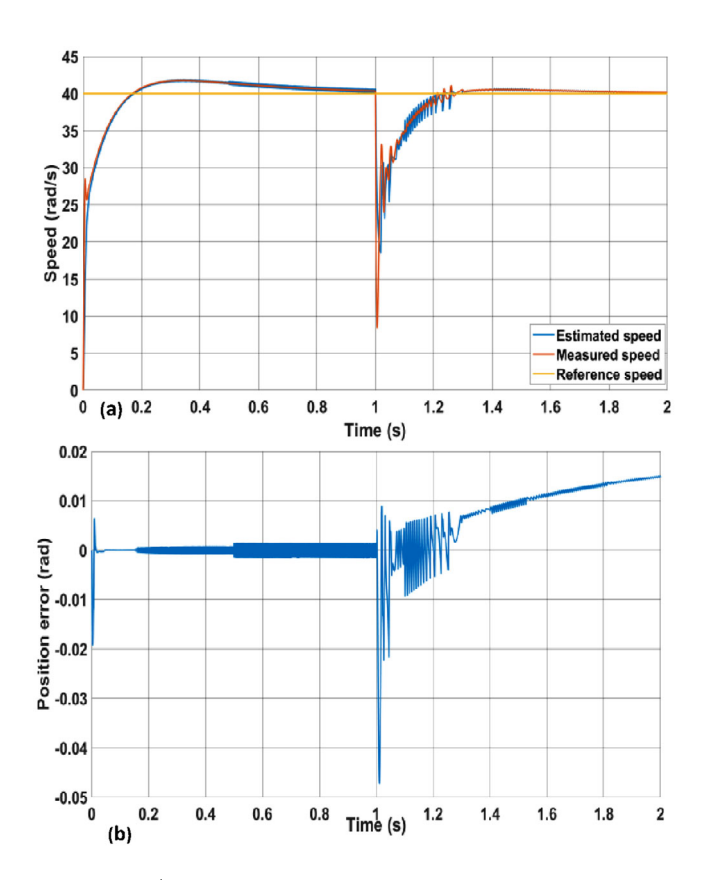


**FIGURE 4** | Predictive method at low speeds, (a) speed, (b) position error.



 $\textbf{FIGURE 5} \quad | \quad \text{Performance at rated torque (a) speed, (b) position error.}$ 

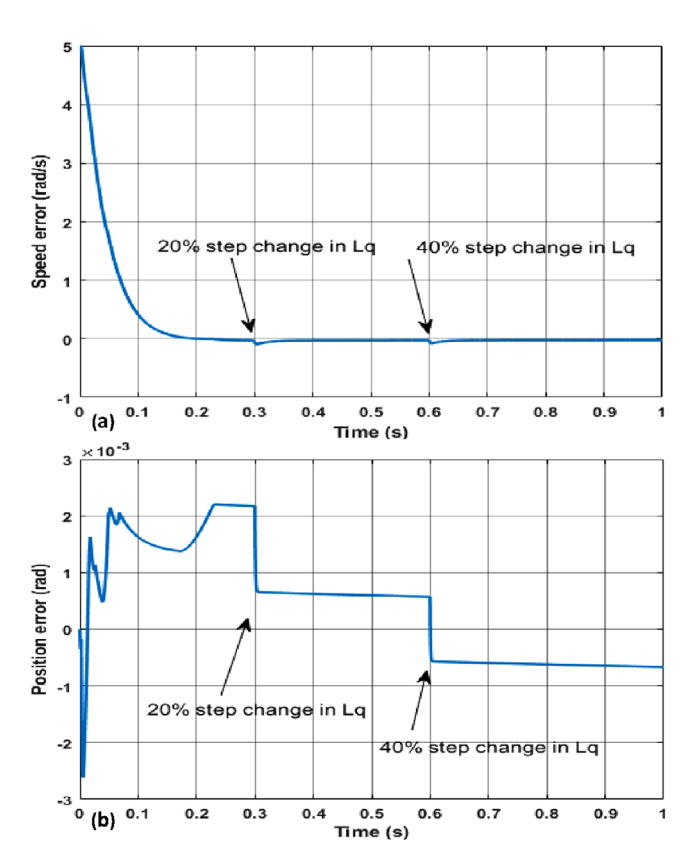


**FIGURE 6** Effect of q-inductance change for the predictive method, (a) speed error, (b) corresponding position error.

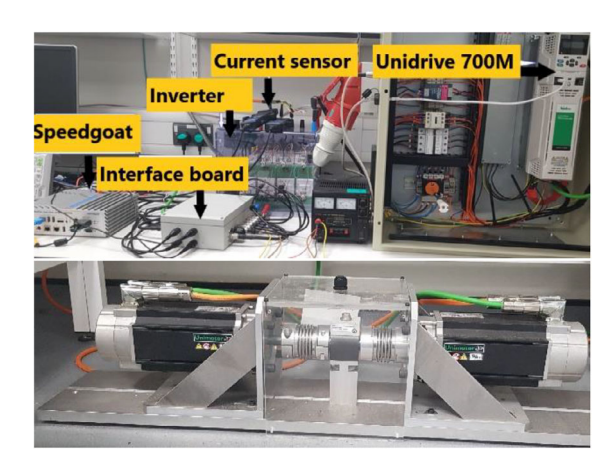
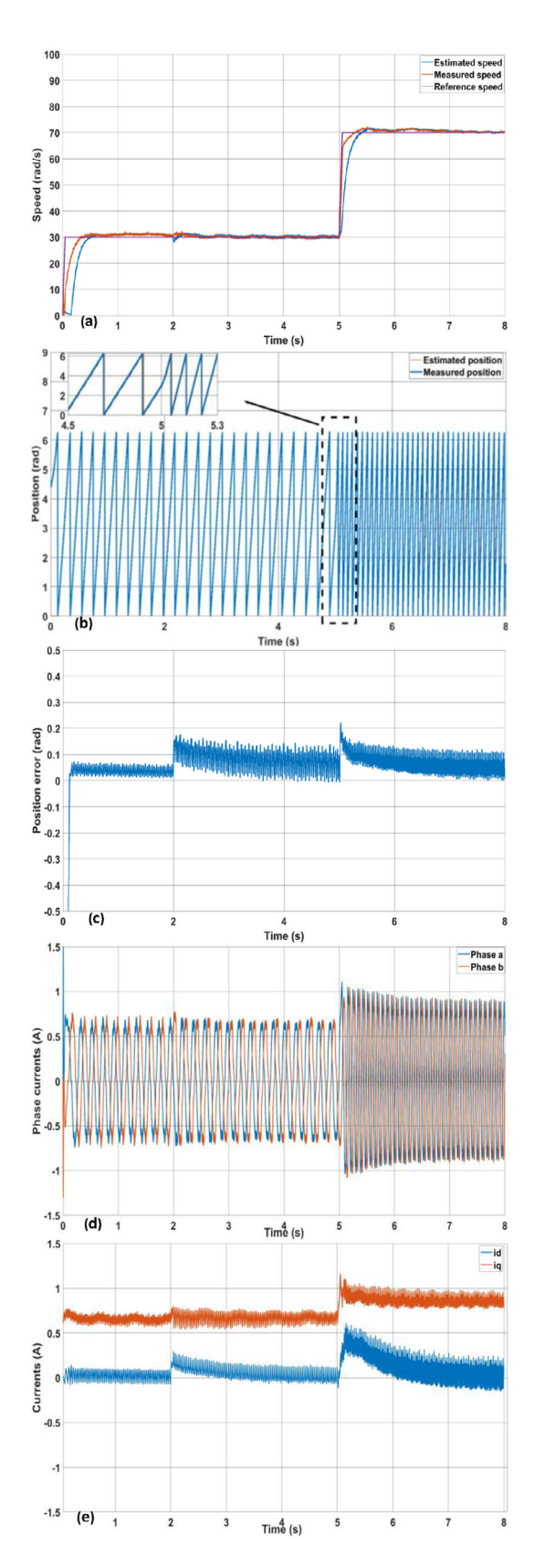


FIGURE 7 | Experimental setup.

back to 5 rad/s as shown in Figure 4a, which means that the motor is properly working in both motoring mode and regenerative mode. From Figure 4b, it can be seen that the position accuracy is not affected even at low speeds Figure 5 shows the performance at rated torque. In Figure 5a, the reference speed is established at 40 rad/s, and the torque is initially set to zero, and then the rated torque is applied at 1 s. It can be noticed that when the torque is applied the estimated speed takes about 0.3s to track the reference speed. Also, the angle error during the transient period does not exceed 0.05 rad as depicted in Figure 5b.

To assess the robustness against variations in motor parameters, the *q*-inductance was changed by 20% at 0.3 s and then by 40%

The Journal of Engineering, 2025 5 of 11



**FIGURE 8** Predictive method performance for sensorless mode, (a) speed response, (b) estimated and measured positions, (b) position error, (d) phase currents, (e) d–q currents.

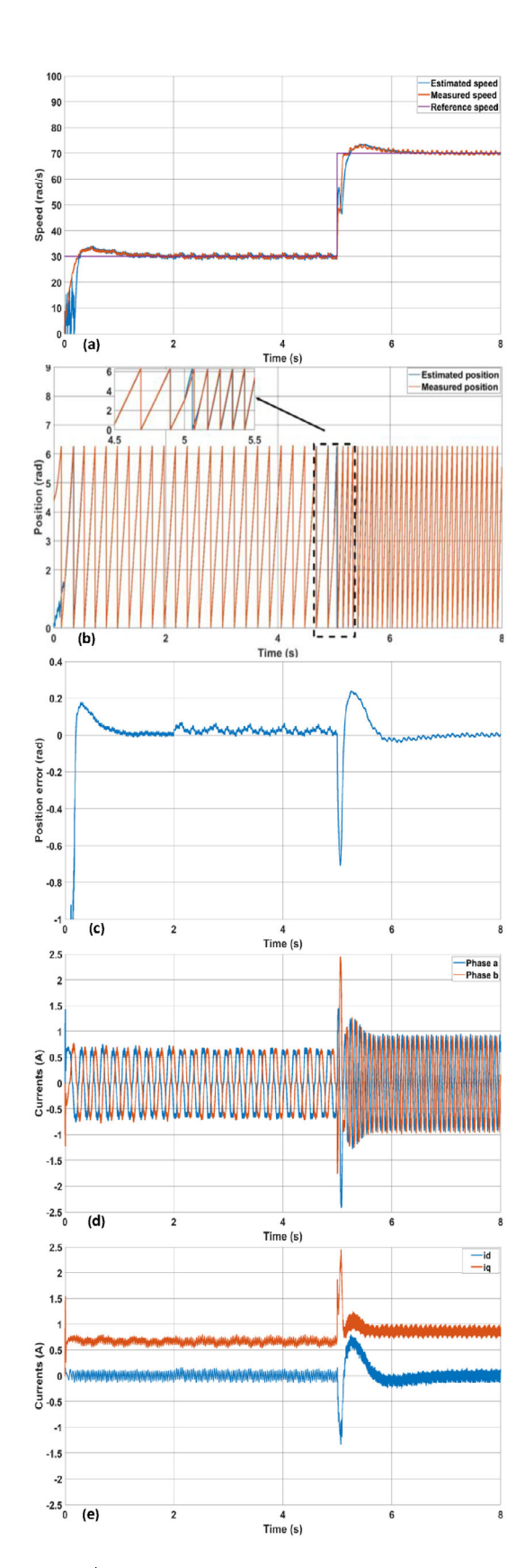


**FIGURE 9** | Conventional method performance for sensorless mode, (a) speed response, (b) estimated and measured positions, (b) position error, (d) phase currents, (e) d–q currents.

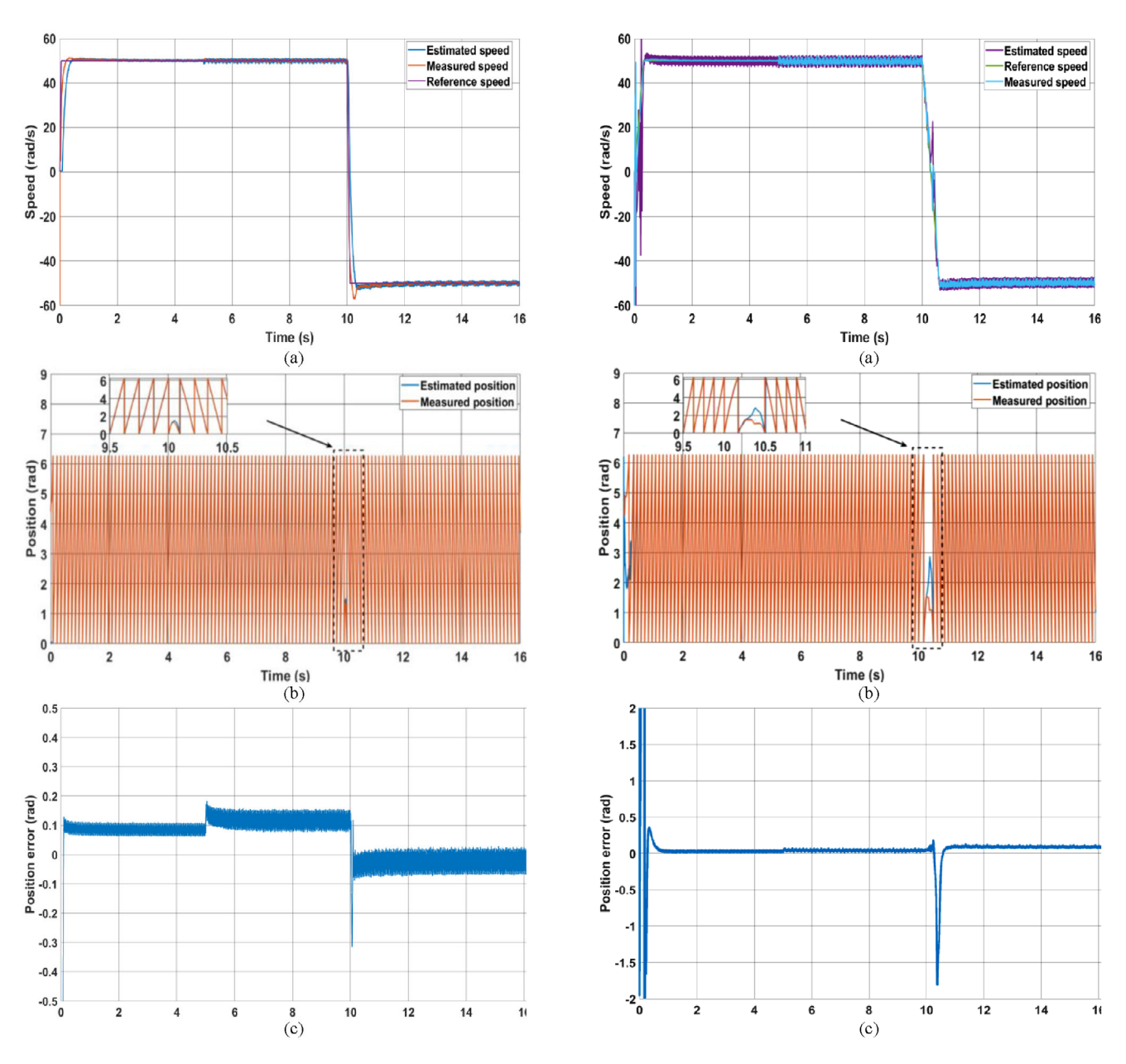


**FIGURE 10** | Reverse speed performance for sensorless mode of the predictive method at no load, (a) speed response, (b) measured and estimated positions, (c) position error.

**FIGURE 11** | Reverse speed performance for sensorless mode of the conventional method at no load, (a) speed response, (b) measured and estimated positions, (c) position error.

as shown in Figure 6. It is clear that both position and speed accuracy remain unaffected by the inductance variation as shown in Figure 6a,b respectively.

## 6 | Experimental Setup

The experimental platform (Figure 7) consists of two identical 2.1 kW PMSMs, each with moderate saliency (saliency ratio 1.2). The motor parameters are presented in Table 1. One is connected to a three-phase two-level inverter (Semikron IGBT module stack) and controlled by a Speedgoat real-time controller. The second drive unit is controlled by a Nidec Unidrive 700 M drive. The two motors can be used in both speed control or torque control modes. A 4096 counts/rev quadrature encoder is used to measure

the rotor position, and two current sensors (TA189) are used for current measurements. The inverter switching frequency is 3.125 kHz with a dead time of 0.5  $\mu$ s, and the control strategy FOC is implemented with a sampling time of 80  $\mu$ s. The PI controller gains of the conventional MRAS are set to  $K_{\rm i>}=200$  and  $K_{\rm i}=1000$  by using the trial-and-error method.

## 7 | Experimental Results

The performance of the proposed estimator is experimentally tested in sensorless mode and compared with the conventional MRAS scheme. In position-sensorless mode of operation, the FOC scheme is driven by the estimated speed. The sensorless performance of the predictive observer shows oscillations in the

The Journal of Engineering, 2025 7 of 11

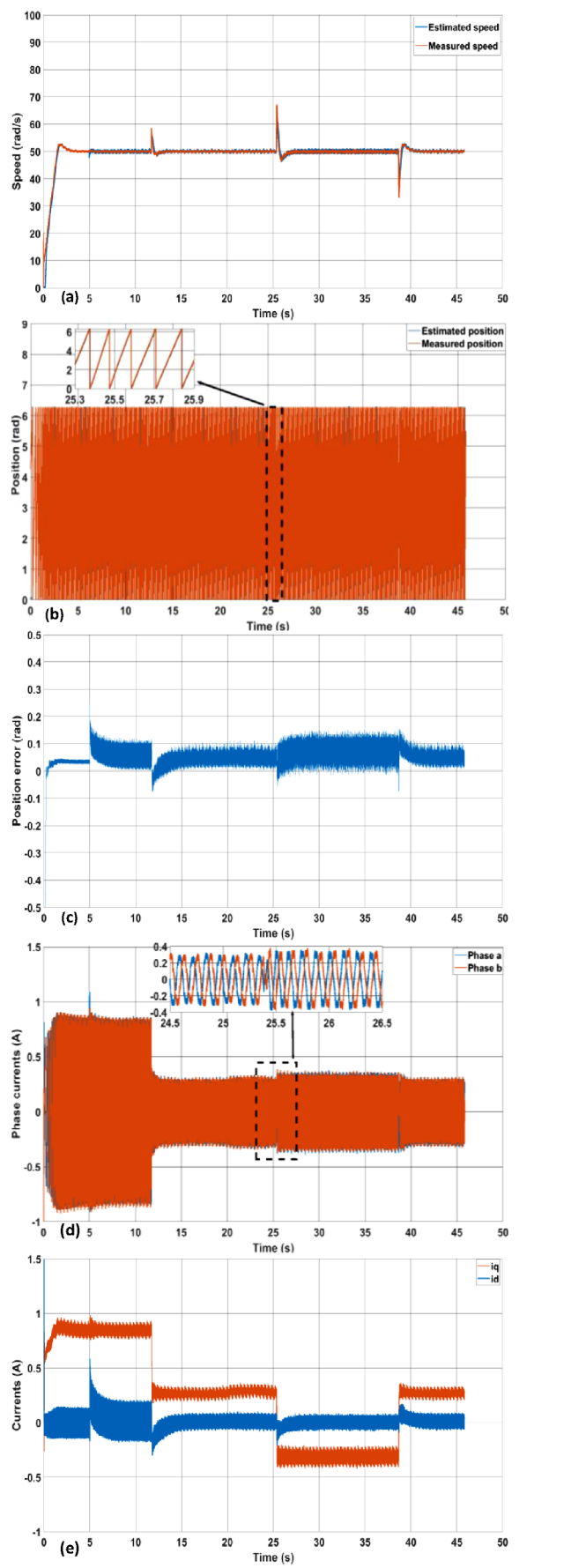


**FIGURE 12** | The predictive method with regenerative mode, (a) speed, (b) positions, (c) position error, (d) phase currents (e) d–q currents.

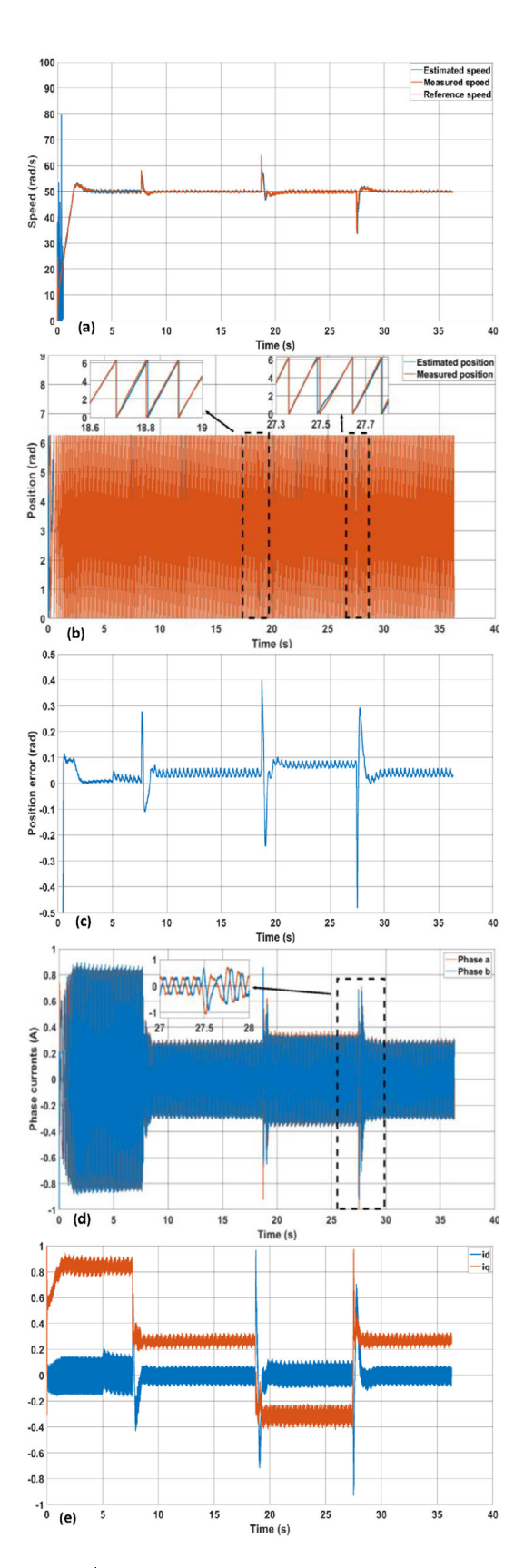


**FIGURE 13** | The conventional method with regenerative mode, (a) speed, (b) positions, (c) position error, (d) Phase currents (e) d-q currents.

**TABLE 2** | Quantitative performance of the two methods.

Metric	Operating point	PI-based MRAS	FCS-MPC
Peak position error	30 to 70 rad/s step	0.7 rad	0.2 rad
	Crossing zero speed	1.7 rad	0.3 rad
	Load step from 30% to 0% of rated load	0.5 rad	0.12 rad
Speed ripples	30 rad/s	3.5%	0.5%
	70 rad/s	1.4%	0.2%
	50 rad/s at 15% of rated load	0.5%	1%
Settling time	30 to 70 rad/s step	0.9s	0.45s
	Step from 30% to 0% of rated load	1.2s	1s
Overshooting	30 to 70 rad/s step	10%	2%
	Step from 0% to 15% of rated load	14%	11%
THD	30 to 70 rad/s step	9.6%	5.7%
Execution time	TI C2000 (150 MHz)	15 μs	39 μs

estimated speed, especially at low speeds. Interestingly, an LPF with a 2 Hz cut-off frequency is tested with the predictive method and successfully reduces the estimated speed oscillations without affecting the running drive even when a disturbance is applied (e.g. speed change). Therefore, an adaptive low-pass filter can be used to reduce the cut-off frequency gradually to the minimum in the steady state for higher filtering quality and set it to 10 Hz for a faster dynamic response during transient operation. It is worth noting that both estimators are combined with open-loop or signal injection methods to switch to sensorless at sufficiently high speeds.

Figures 8 and 9 show the performance of the two methods in sensorless mode at 2 s when the reference speed is changed from 30 to 70 rad/s at no load. In Figures 8a and 9a, it is evident that the predictive estimator provides a more accurate estimation of speed, especially at lower speeds. Moreover, Figures 8b,c and 9b,c show that the angle error during the transient period is lower for the predictive method, at nearly 0.21 rad, compared to about -0.7 rad for the classical method. This can be noticed from the currents produced by the two methods during the transient period which are higher in the classical method compared to the predictive method as shown in Figures 8d,e and 9d,e.

Figures 10 and 11 show the two methods' performance for sensorless operation at 5 s when the reference speed crosses zero, representing the reverse speed response from positive to negative speed at no load. In Figure 10a, it is shown that the drive can cross zero speed with a smoother response during the transient period compared to the conventional method. In the conventional method, a speed rate limiter is needed for a smooth transient response, as seen in Figure 11a. The position error produced by the predictive method during the transient period is about -0.3 rad compared to about -1.8 rad with the conventional method, as shown in Figures 10b,c and 11b,c, respectively.

Figures 12 and 13 show the classical and predictive performance in the regenerative mode for sensorless operation at 5 s. At the speed reference of 50 rad/s, 15% of the rated load is applied initially, followed by an increase to 30% of the rated torque, and finally a

fall to 15% as shown in Figures 12a and 13a. It is shown that the speed oscillation slightly increases, and the position error does as well for both methods. During the transient period, the position error increases significantly in the conventional method when the load changes, while in the predictive scheme, the error increases only slightly, as shown in Figures 12b,c and 13b,c. This is clearly demonstrated in Figures 12d,e and 13d,e, which show that the current is almost unaffected during the transient period in the predictive method, while it increases significantly in the classical method.

Table 2 presents a comparative experimental analysis between the classical flux-based MRAS and the proposed PWM-based MRAS under identical test conditions. It achieves lower peak position error during transients, reduced speed ripple, faster settling times, and significantly smaller overshoot values. For example, during a speed step from 30 to 70 rad/s, the position error decreases from 0.7 to 0.2 rad, the overshoot from 10% to 2%, and the THD from 9.6% to 5.7%. The only case where PI-based MRAS shows an advantage is at light-load operation (50 rad/s, 15% load), where it achieves slightly lower speed ripple. Overall, FCS-MPC demonstrates better dynamic performance.

## 8 | Conclusion

In this paper, a predictive speed estimator is implemented for the proposed PWM-based estimator. The estimator is based on the FCS-MPC principle to minimize the speed tuning error signal of the MRAS scheme and eliminate the PI controller in the speed estimator. The experimental results show that the speed oscillation at low speeds can be significantly reduced with the predictive estimator by using an LPF with a very low cut-off frequency without affecting the system performance, in comparison with the classical MRAS. In addition, during the transient period, the predictive scheme demonstrates a significantly lower position error during fast load transients compared to the conventional PI-based MRAS scheme. The proposed estimator operates over an adjustable speed range from below 5 rad/s, since no integrator is used in the voltage model of MRAS, up to  $\pm 944$  rad/s electrical

The Journal of Engineering, 2025

(rated speed). However, because the command voltages generated by the controller are used instead of the measured voltages, inverter nonlinearity and dead-time effects are not considered. At very low speeds, these effects become more pronounced, leading to noticeable speed oscillations. Therefore, compensation strategies for inverter nonlinearity and dead-time effects should be investigated in future work to improve accuracy in this operating region. Moreover, according to [24], the PI-based MRAS estimator has demonstrated satisfactory performance for id  $\neq 0$ , confirming its ability to operate in the flux-weakening region. Notably, [24] employed the same motor as in this paper, a surface-mounted permanent magnet (SPM) synchronous motor with moderate saliency. Accordingly, it is recommended that the predictive method presented in this paper also be extensively tested on PMSMs under flux-weakening conditions to further validate its robustness.

#### **Author Contributions**

**Saleh B. Shlimet:** data curation, formal analysis, investigation, methodology, software, validation, visualization, writing – original draft. **Antonio Griffo:** conceptualization, funding acquisition, project administration, resources, supervision, writing – review and editing.

#### **Funding**

This research was funded by the Libyan embassy in London, UK during the PhD.

#### **Conflicts of Interest**

The authors declare no conflicts of interest.

# Data Availability Statement

The data presented in this study are available in the article.

#### References

- 1. R. Krishnan, Permanent Magnet Synchronous and Brushless DC Motor Drives (CRC Press, 2017).
- 2. J.-H. Im and R.-Y. Kim, "Improved Saliency-Based Position Sensorless Control of Interior Permanent-Magnet Synchronous Machines with Single DC-Link Current Sensor Using Current Prediction Method," *IEEE Transactions on Industrial Electronics* 65, no. 7 (2018): 5335–5343, https://doi.org/10.1109/TIE.2017.2777382.
- 3. M. Rashed and A. F. Stronach, "A Stable Back-EMF MRAS-Based Sensorless Low-Speed Induction Motor Drive Insensitive to Stator Resistance Variation," *IEE Proceedings—Electric Power Applications* 151, no. 6 (2004): 685–693, https://doi.org/10.1049/ip-epa:20040609.
- 4. S. M. Gadoue, D. Giaouris, and J. W. Finch, "MRAS Sensorless Vector Control of an Induction Motor Using New Sliding-Mode and Fuzzy-Logic Adaptation Mechanisms," *IEEE Transactions on Energy Conversion* 25, no. 2 (2010): 394–402, https://doi.org/10.1109/TEC.2009. 2036445.
- 5. M. Comanescu, "An MRAS-Type Estimator for the Speed Flux Magnitude and Rotor Flux Angle of the Induction Motor Using Sliding Mode." in 2014 International Symposium on Power Electronics, Electrical Drives, Automation and Motion (Speedam) (IEEE, 2014), 719–724.
- 6. M. A. Khoshhava, H. A. Zarchi, and G. A. Markadeh, "Sensor-Less Speed and Flux Control of Dual Stator Winding Induction Motors

- Based on Super Twisting Sliding Mode Control," *IEEE Transactions on Energy Conversion* 36 (2021): 3231–3240, https://doi.org/10.1109/TEC.2021. 3077829.
- 7. S. A. Mansouri, A. Ahmarinejad, M. S. Javadi, R. Heidari, and J. P. S. Catalão, "Improved Double-Surface Sliding Mode Observer for Flux and Speed Estimation of Induction Motors," *IET Electric Power Applications* 14 (2020): 1002–1010, https://doi.org/10.1049/iet-epa.2019.0826.
- 8. A. Farahat, Z. Liu, G. Liu, and Q. Chen, "Speed and Position Estimation for 5-ph PMSM Using SOGI Based on SMO Considering Short-Circuit Fault," *IEEE Access* 12 (2024): 57315–57325, https://doi.org/10.1109/ACCESS.2024.3387284.
- 9. T. Wang, B. Wang, Y. Yu, and D. Xu, "A Closed Loop Voltage Model Observer for Sensorless Induction Motor Drives Based on the Orthogonality and Sliding-Mode Technique," *IEEE Transactions on Industrial Electronics* 71 (2024): 13693–13707, https://doi.org/10.1109/TIE. 2024.3374363.
- 10. W. Liu, B. Luo, Y. Yang, et al., "An Adaptive-Gain Sliding Mode Observer With Precise Compensation for Sensorless Control of PMSM," *Energies* 16, no. 24 (2023): 7968, https://doi.org/10.3390/en16247968.
- 11. Z. Shen, Z. Yang, X. Sun, and W. Pan, "Sensorless Control of Bearingless Induction Motor Based on Fuzzy Dual Sliding Mode MRAS," *Electrical Engineering* 107 (2025): 5737–5747, https://doi.org/10.1007/s00202-024-02835-5.
- 12. X. Peng, X. Wang, H. Li, and F. Cao, "Sensorless Control of PMSM Based on Fuzzy Integral Terminal Sliding Mode Observer," *Journal of Electrical Systems* 21, no. 1 (2025): 572–580.
- 13. L. Zhang, R. Tao, J. Bai, and D. Zeng, "An Improved Sliding Mode Model Reference Adaptive System Observer for PMSM Applications," *Expert Systems with Applications* 250 (2024): 123907, https://doi.org/10.1016/j.eswa.2024.123907.
- 14. K. M. S. Benzaoui, E. Benyoussef, and A. Z. Kouache, "Artificial Neural Network Sensorless Direct Torque Controlof Two Parallel-Connected Five-Phase Induction Machines," *Majlesi Journal of Electrical Engineering* 18, no. 3 (2024): 1–14.
- 15. S. Saeidi and R. Kennel, "A Novel Algorithm for Model Predictive Control of AC Electric Drives," in IEEE 2nd International Electric Drives Production Conference (IEEE, 2012), 78–84.
- 16. S. Nalakath, Y. Sun, M. Preindl, and A. Emadi, "Optimization-Based Position Sensorless Finite Control Set Model Predictive Control for IPMSMs," *IEEE Transactions on Power Electronics* 33, no. 10 (2018): 8672–8682, https://doi.org/10.1109/TPEL.2017.2784816.
- 17. J. Guzinski and H. Abu-Rub, "Speed Sensorless Induction Motor Drive With Predictive Current Controller," *IEEE Transactions on Industrial Electronics* 60, no. 2 (2013): 699–709, https://doi.org/10.1109/TIE.2012. 2205359.
- 18. J. L. Chen and T. H. Liu, "Implementation of a Predictive Controller for a Sensorless Interior Permanent-Magnet Synchronous Motor Drive System," *IET Electric Power Applications* 6, no. 8 (2012): 513–525, https://doi.org/10.1049/iet-epa.2011.0242.
- 19. R. Vargas, J. Rodriguez, C. A. Rojas, and M. Rivera, "Predictive Control of an Induction Machine Fed by a Matrix Converter with Increased Efficiency and Reduced Common-Mode Voltage," *IEEE Transactions on Energy Conversion* 29, no. 2 (2014): 473–485.
- 20. L. Tong, X. Zou, S. Feng, et al., "An SRF-PLL-Based Sensorless Vector Control Using the Predictive Deadbeat Algorithm for the Direct-Driven Permanent Magnet Synchronous Generator," *IEEE Transactions on Power Electronics* 29, no. 6 (2014): 2837–2849, https://doi.org/10.1109/TPEL.2013. 2272465.
- 21. Y. B. Zbede, S. M. Gadoue, and D. J. Atkinson, "Model Predictive MRAS Estimator for Sensorless Induction Motor Drives," *IEEE Transactions on Industrial Electronics* 63, no. 6 (2016): 3511–3521, https://doi.org/10.1109/TIE.2016.2521721.

- 22. S. Xiao and A. Griffo, "PWM-Based Flux Linkage Estimation for Permanent Magnet Synchronous Machines," *Journal of Engineering* 2019, no. 17 (2019): 4045–4049.
- 23. M. Shiref, Investigation Into PI Controller Output Ripple in MRAS Based Electrical Drives (Newcastle University, 2013).
- 24. S. B. Shlimet and A. Griffo, "PWM-Based Speed and Position Estimations for Permanent Magnet Synchronous Machines," *Applied Sciences* 15, no. 18 (2025): 9859, https://doi.org/10.3390/app15189859.

The Journal of Engineering, 2025